Available online at www.sciencedirect.com
ScienceDirect
Aerosol Science 39 (2008) 348–364
Journal of Aerosol Science
www.elsevier.com/locate/jaerosci

Method to measure time-dependent scattering cross sections of particles evaporating in a laser beam

Nobuhiro Moteki*, Yutaka Kondo

Research Center of Advanced Science and Technology, University of Tokyo, Room-414 Bldg.-3, 4-6-1, Komaba, Meguro-ku, Tokyo 153-8904, Japan

Received 6 September 2007; received in revised form 3 December 2007; accepted 3 December 2007

Abstract

We develop a new method of measuring the time-dependent solid angle scattering cross section for detection ($\Delta C_{sca}(t)$) of individual particles flowing across a Gaussian laser beam. This method is based on the principle that the normalized derivative of the scattering signal (S'/S) measured by an instrument can be decomposed into the normalized derivative of the incident irradiance (I'/I) and that of the scattering cross section ($\Delta C'_{sca}/\Delta C_{sca}$). For evaporative particles, $S'/S = I'/I$ holds true until evaporation starts at a certain position in the laser beam. The $I(t)$ for individual particles is determined from I'/I, which is extracted from S'/S. $\Delta C_{sca}(t)$ is derived from $I(t)$ and $S(t)$. We apply the method to particles with and without evaporation using a single-particle soot photometer. The robustness of the method is confirmed through results for non-evaporative particles. For evaporative particles, derived ΔC_{sca} values before the onset of evaporation are compared to Mie theory.

Keywords: Particle sizing; Light scattering; Single-particle; Evaporation

1. Introduction

Laser light scattering has for a long time been one of the most widely used techniques for measuring the size of aerosols (Kerker, 1997). Generally, scattering probes measure the differential scattering cross section integrated over angular ranges of scattered light collection for individual particles and convert it to particle size assuming particle refractive index and shape. Hereafter, we denote the "differential scattering cross section of a particle integrated over the solid angle of light collection" as ΔC_{sca}. Most commercially available scattering probes determine the size of flowing individual particles by the peak amplitude of the scattering signal, which is proportional to the ΔC_{sca} of the particle (e.g., Pinnick, Pendleton, & Videen, 2000). Using a high-power probing laser or the long-time illumination of the particle to achieve a low limit of detection may raise a fundamental problem in the measurements. Specifically, if the particle shrinks in the laser beam by evaporation due to heating, the ΔC_{sca} determined from the peak amplitude of the scattering signal is underestimated. Particles consisting of light-absorbing compounds (e.g., carbonaceous, metals) in particular are expected to be subject to this problem. Recently, intra-cavity, high-power probing lasers have become widely used as light sources for optical particle counters, detecting fine particle down to sub-0.1-μm diameters (Pinnick et al., 2000; Schuster & Knollenberg, 1972). To our knowledge, however, the possible effects of evaporation of light-absorbing

* Corresponding author. Tel.: +81 3 5452 5147; fax: +81 3 5452 5148.
E-mail address: moteki@atmos.rcast.u-tokyo.ac.jp (N. Moteki).

0021-8502/$ - see front matter © 2007 Elsevier Ltd. All rights reserved.
doi:10.1016/j.jaerosci.2007.12.002

particles have not been taken into account thus far. The laser-induced incandescence (LII) technique, which utilizes a high-power probing laser, is widely used for the detection and physical characterization of soot particles (Schulz et al., 2006). By using the LII technique, the ΔC_{sca} of soot particles internally mixed with evaporative compounds (e.g., sulfate, organics) cannot be measured because of the particle evaporation problem denoted above (Schwarz et al., 2006). Gao et al. (2007) proposed a method to estimate the ΔC_{sca} of soot-containing particles prior to evaporation by adding a position-sensitive detector to the LII instrument for scattered light detection. The measurement of the evaporation rate of individual aerosols in the laser beam is becoming important in order to validate physical models describing laser-induced evaporation phenomena of aerosol particles (e.g., Schoolcraft, Constable, Zhigilei, & Garrison, 2000; Sleicher & Churchill, 1956).

We have developed a new method to measure the time-dependent ΔC_{sca} of individual particles in a laser beam. For this study, we used conventionally instrumented scattering probes using a Gaussian continuous-wave (i.e., TEM_{00} mode) laser. This method estimates the center position and width of the Gaussian function of incident laser irradiance $I(t)$ from the normalized time derivative (i.e., rate of change) of the scattering signal. Using $I(t)$, we can estimate the $\Delta C_{sca}(t)$ of individual particles, including ΔC_{sca} before the onset of evaporation. This method can be applied for the accurate correction of the underestimation of optical particle sizing due to particle evaporation.

2. Measurement system

In this section we describe instrumental configurations of scattering probes to which our new method to measure $\Delta C_{sca}(t)$ can be applied. Fig. 1 shows a schematic diagram of a scattering probe measuring the waveform of scattering intensity of flowing particles. A Gaussian continuous-wave laser beam is used as a light source for particle irradiation. The aerosol flow intersects with the laser beam at right angles. The light elastically scattered by a transiting particle is assumed to be collected with constant efficiency over all angles where the particle is irradiated by the laser beam. The width of the laser beam is much wider than that of the aerosol flow such that particles always pass through the

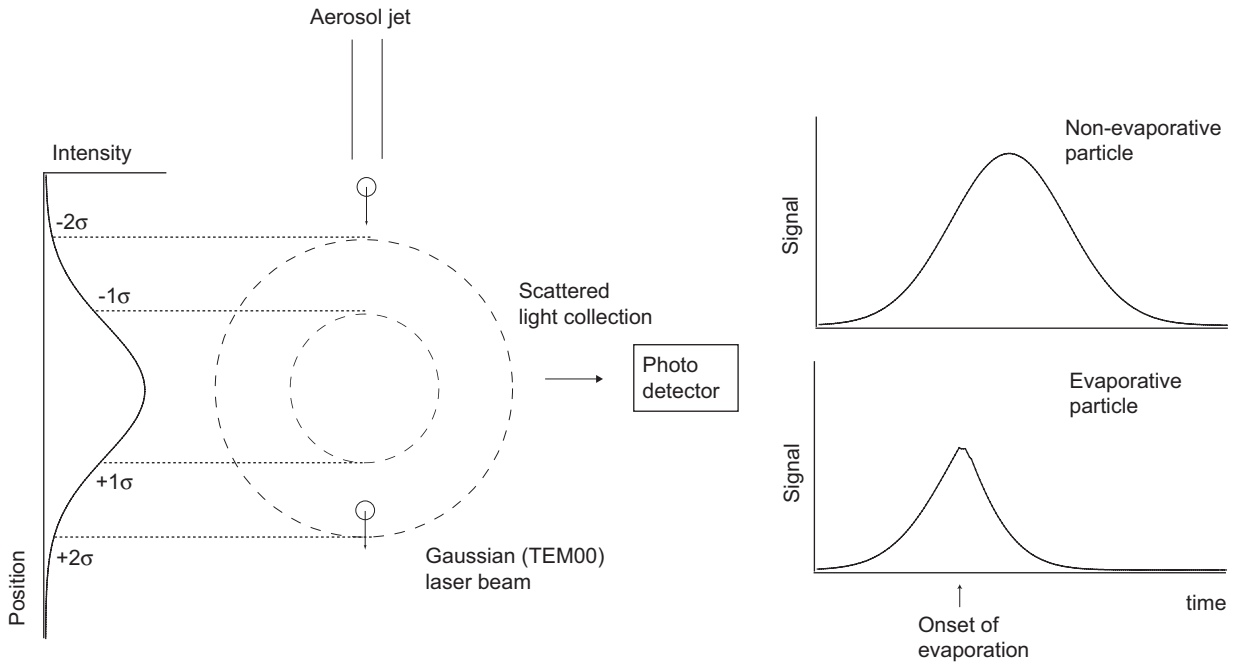

Fig. 1. General schematic diagram of the scattering probe for sizing individual flowing particles using a continuous-wave Gaussian laser beam. The aerosol particles intersect with the laser beam at right angles with constant velocity. Conceptual waveforms of the scattering signal of a particle with and without evaporation are also shown on the right-hand side of the figure. The waveform of the scattering signal for non-evaporative particle becomes Gaussian in shape, which is equal to the cross-sectional profile of the Gaussian (TEM_{00} mode) laser beam. In contrast, the corresponding waveform for the evaporative particle is distorted from the Gaussian function because of evaporation of the particle during transit in the laser beam.

cross-sectional center of the laser beam. The particle transit velocity only depends on the flow rate of the carrier gas in the aerosol jet and does not depend on any other factors (e.g., particle size, effects of laser irradiation). The time-dependent signal intensity of elastically scattered light is measured and stored with a sampling interval much (i.e., orders of magnitude) shorter than the particle's residence time in the laser beam.

The incident irradiance $I(t)$ of the laser beam for individual particles is described by a Gaussian function with respect to elapsed time t,

$$I(t) = I_0 \exp\left(-\frac{(t-\tau)^2}{2\sigma^2}\right), \tag{1}$$

where I_0, τ, and σ denote incident irradiance at the cross-sectional center of the beam, center time, and 1-standard deviation (width) of the Gaussian function, respectively. The measured signal ($S(t)$) of elastically scattered light by individual aerosols is proportional to the product of $I(t)$ and the $\Delta C_{\mathrm{sca}}(t)$ of the particle,

$$S(t) = sI(t)\int_{\Delta\Omega}\left(\frac{\mathrm{d}C_{\mathrm{sca}}}{\mathrm{d}\Omega}\right)\mathrm{d}\Omega = sI(t)\Delta C_{\mathrm{sca}}(t), \tag{2}$$

where s denotes a proportionality constant that depends on the instrument, and $\Delta\Omega$ denotes the solid angle of light collection. As schematically shown in Fig. 1, for non-evaporative (i.e., non-light-absorbing) particles, $S(t)$ becomes a Gaussian function because ΔC_{sca} does not change with time during laser irradiation. In contrast, for evaporative (i.e., light-absorbing) particles, ΔC_{sca} changes due to evaporation of the particle inside the laser beam, and $S(t)$ deviates from the Gaussian function after the onset of evaporation. From Eqs. (1) and (2), the time-dependent scattering cross section $\Delta C_{\mathrm{sca}}(t)$ of the particle can be written as

$$\Delta C_{\mathrm{sca}}(t) = \frac{1}{s}\cdot\frac{S(t)}{I(t)} = \frac{1}{sI_0}\cdot S(t)\cdot\exp\left\{\frac{(t-\tau)^2}{2\sigma^2}\right\}, \tag{3}$$

where $1/sI_0$ is an instrument-dependent constant that is calibrated by measuring the peak amplitude of the scattering signal (i.e., $S(t=\tau)$) of non-evaporative particles with known ΔC_{sca}. In this study, the value of $1/sI_0$ in Eq. (3) equals 1.22×10^{-17} ($\mathrm{m}^2/2.44\,\mathrm{mV}$). For evaporative particles, $\Delta C_{\mathrm{sca}}(t)$ can be determined from measured $S(t)$ by Eq. (3) if both the center (τ) and width (σ) of the Gaussian function are known.

In this study, we use a single-particle soot photometer (SP2) (Droplet Measurement Technology, Inc., Boulder, CO) as the scattering probe. The principle and configuration of the SP2 have already been fully described by others (Baumgardner, Kok, & Raga, 2004; Gao et al., 2007; Moteki & Kondo, 2007; Schwarz et al., 2006; Slowik et al., 2007; Stephens, Turner, & Sandberg, 2003). In this study, configurations and operating conditions of the SP2 are almost the same as those described in Moteki and Kondo (2007). The SP2 uses an intra-cavity Nd:YAG laser with a wavelength of 1064 nm and records $S(t)$ with a data sampling rate of 5 MHz (i.e., every 0.2 μs). The $S(t)$ is digitized with 12-bit resolution ranging from −5 to +5 V (2.44-mV resolution). Hereafter, we always denote t and $S(t)$ in units of 0.2 μs and 2.44 mV, respectively. Scattered light is collected over a solid angle of $\sim \pi/2$ sr around scattering angles of 45° and 135°. The incident irradiance at the center of the Gaussian I_0 (in Eq. (1)) is $\sim 10^6\,\mathrm{W\,cm^{-2}}$. The $1/e^2$ power diameter of the laser beam is about 1 mm. The detectable range of particle diameters (D_{p}) for the SP2 is approximately 200–1000 nm for particles with optical properties equivalent to those of polystyrene latex. The width of the Gaussian function (σ) is about 3–4 μs, which depends on the ratio of the beam diameter to the flow rate of the carrier gas in the aerosol jet. Because the aerosol jet flow is driven by a diaphragm pump with a motor frequency of 50 Hz, the flow rate suffers from 50-Hz fluctuation, with an amplitude of about 8%. Because the time-cycle of the flow fluctuation is 3 orders of magnitude longer than the particle transit time (i.e., width of Gaussian), the shape of the Gaussian function (Eq. (1)) for individual particles is not distorted by the flow fluctuation. In addition to the scattering signal, the laser-induced incandescence signal in the visible band($\lambda = 350$–800 nm) is simultaneously measured by the SP2. Only particles that consist of refractory carbon (e.g., graphite, glassy carbon) or metals emit LII signals detectable by the SP2, because of their efficient light absorption and high boiling points ($T > \sim 10^3$ K) (Schwarz et al., 2006).

3. Theoretical framework

As described in the previous section, the two unknown parameters in the Gaussian function, namely the τ and the σ in Eq. (1), need to be determined in order to estimate the $\Delta C_{\mathrm{sca}}(t)$ of evaporative particles. We introduce a new method to estimate the parameters of the Gaussian function for evaporative particles. This method is innovative in that it uses a normalized time derivative (i.e., rate of change) of the scattering signal $S'(t)/S(t)$ instead of the scattering signal $S(t)$ itself. From Eq. (2), the normalized derivative of $S(t)$ (i.e., S'/S) can be decomposed into the normalized derivative of $I(t)$ (i.e., I'/I) and the normalized derivative of ΔC_{sca} (i.e., $\Delta C'_{\mathrm{sca}}/\Delta C_{\mathrm{sca}}$) as follows:

$$\frac{S'}{S}(t) = \frac{I' \cdot \Delta C_{\mathrm{sca}} + I \cdot \Delta C'_{\mathrm{sca}}}{I \cdot \Delta C_{\mathrm{sca}}} = \frac{I'}{I}(t) + \frac{\Delta C'_{\mathrm{sca}}}{\Delta C_{\mathrm{sca}}}(t). \tag{4}$$

If ΔC_{sca} is not changed by evaporation or any other laser-induced change of optical properties of the particle, S'/S is equal to I'/I. The I'/I of the Gaussian beam (i.e., TEM_{00} mode) is derived from Eq. (1) as

$$\frac{I'}{I}(t) = -\frac{1}{\sigma^2}(t - \tau). \tag{5}$$

Eq. (5) shows that I'/I is a linear function of t, whose slope and intercept are related to the center (τ) and width (σ) of the Gaussian function. The I'/I ratio equals 0 at the center of the Gaussian ($t = \tau$).

Fig. 2a shows an $S(t)$ waveform measured by the SP2 for a non-evaporative particle (polystyrene latex) and calculated S'/S. The time derivative of scattering signal S' is numerically calculated from the $S(t)$ data (Appendix A.1). The solid line in Fig. 2a represents Eq. (5), with the τ and σ determined by direct nonlinear fitting of a Gaussian function onto the $S(t)$ data. Good agreement between the S'/S data points and Eq. (5) over the entire t-domain is consistent with Eqs. (4) and (5).

As demonstrated later, even strongly evaporative particles do not necessarily begin shrinking just after entering the laser beam. Fig. 2b shows $S(t)$ and S'/S for an evaporative particle (oil-coated graphite). Details of the evaporative particles used in this study will be described in Section 6. From this figure, it is expected that $\Delta C'_{\mathrm{sca}} = 0$ (i.e., $S'/S = I'/I$) at the leading edge ($60 < t < 80$), considering that the data points of S'/S linearly correlate with t very tightly in the t-domain. The dashed line in Fig. 2b is a tentative fit to S'/S at $60 < t < 80$. The slope of the dashed line agrees well with that of the I'/I line in Fig. 2a, supporting the expectation that $\Delta C'_{\mathrm{sca}} = 0$ at the leading edge of $S(t)$.

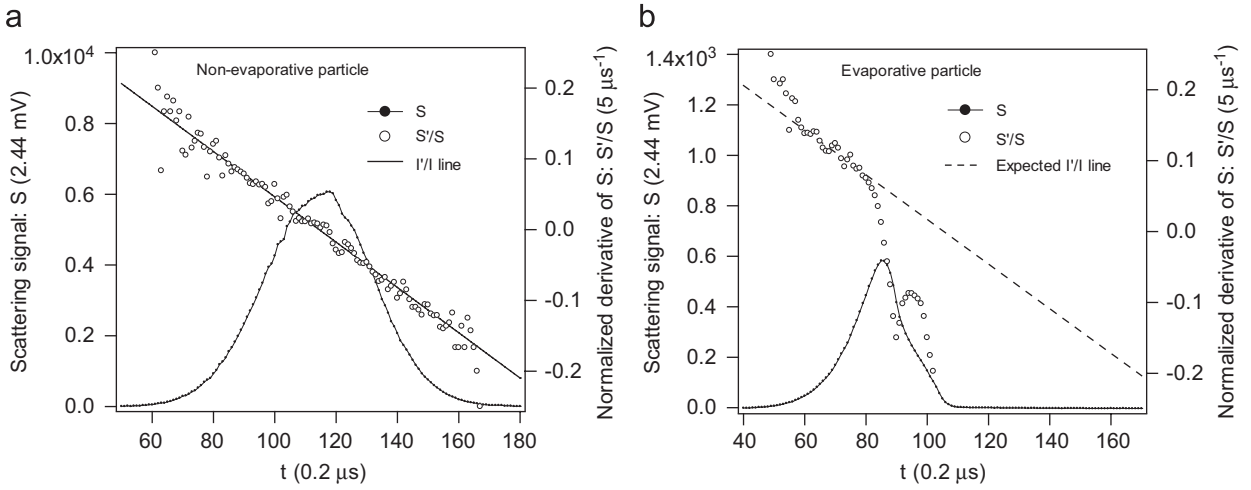

Fig. 2. Scattering signal (S) and normalized derivative of scattering (S'/S) observed for individual particles with and without evaporation. (a) Non-evaporative particle: polystyrene latex (PSL). (b) Evaporative particle: oil-coated graphite. The solid line in (a) indicates the I'/I function whose intercept and slope were determined by direct Gaussian function fitting of the $S(t)$ data. The solid line in (b) is the tentatively fitted I'/I line for the S'/S data segment at the leading edge ($60 < t < 80$).

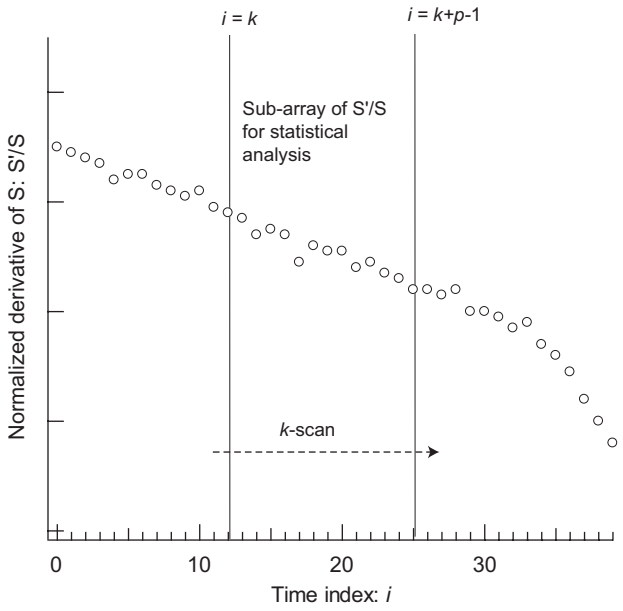

Fig. 3. Schematic for the procedure of I'/I line extraction from the S'/S data segment. The significance of each S'/S data segment is evaluated by the statistical method described in the text.

For evaporative particles, if the I'/I line is correctly determined from a sub-array of S'/S data in a t-domain where $\Delta C'_{\mathrm{sca}} = 0$ holds, the center (τ) and width (σ) of the Gaussian function can be determined from the intercept and slope of the I'/I line. Here we show a mathematical method by which the I'/I line is automatically determined from a sub-array of S'/S. Fig. 3 shows a schematic of the method. We first consider the kth set of continuous data points p of S'/S (i.e., sub-array of S'/S). Here, the optimal number of p points has to be subjectively determined by a trade off between the sample number for statistical analysis and the number of available data points. An appropriate statistical analysis is then conducted to evaluate the reliability of the estimation of the I'/I line using this sub-array of S'/S. The same procedure is iterated for each k, which is scanned from 0 to k_{end}. The appropriate value of k_{end}, namely the upper limit of the k-scan, depends on the measurement system and should be subjectively determined. The best position of the S'/S sub-array (best k) is selected based on an appropriate measure of statistical significance. Finally, the I'/I line is determined from the sub-array of S'/S at the best position.

A simple method for the statistical analysis is the least-squares fitting of the I'/I linear function (Eq. (5)) onto the S'/S sub-array. The values of τ and σ can be calculated from the intercept and slope of the fitted line. However, this method does not work if the S'/S data with $\Delta C'_{\mathrm{sca}} \neq 0$ are tightly linearly correlated with t (e.g., see $85 < t < 100$ in Fig. 7a). Namely, it is possible that the simultaneous determination of both slope and intercept with least-squares fitting leads to an erroneous I'/I line.

If the Gaussian width (σ) of $I(t)$ does not vary particle by particle, the slope of the I'/I line can be constrained to be constant. In this case, only the center of the Gaussian (τ) is determined from the intercept of the I'/I line (Eq. (5)) fitted onto S'/S. The constraint of the slope in the least-squares fitting excludes the erroneous I'/I line. The assumption of a constant σ is acceptable if the fluctuation of the flow rate of the aerosol jet is very small.

For the operating conditions of the instrument in this study, the particle-by-particle variation (1-standard deviation) of the Gaussian width (σ) is 8%. We take into account the particle-by-particle variation of σ in the calculations, because it is difficult to judge objectively whether a fluctuation of 8% is negligible for the purpose of estimating $\Delta C_{\mathrm{sca}}(t)$. In future studies, the assumption of constant σ could be used for the S'/S analysis by improving the stability of the flow rate of the aerosol jet.

The algorithm we adopted in this study provides step-by-step determinations of the two Gaussian parameters. This method excludes erroneous determinations of the I'/I line, in contrast to simultaneous determination of the two parameters. First, we determine the center position of the Gaussian τ for every sub-array of S'/S by a maximum-likelihood

method (Bevington & Robinson, 2003). Simultaneously, the statistical significances of all sub-arrays of S'/S ($k=0 \sim k_{\mathrm{end}}$) are evaluated by their statistical distance (Johnson & Wichern, 2007; Mahalanobis, 1936). Then, based on the statistical significance of each sub-array, the best estimate of τ for the particle is determined. Finally, the width of the Gaussian σ is determined by least-squares fitting of a linear function with a priori knowledge of τ. Details of the algorithm are described in Appendix A.

4. Determination of the I'/I line

4.1. General features

Before applying the method to evaporative particles, we have to characterize the I'/I line of the instrument. For this purpose, we analyze measured signals of non-evaporative polystyrene latex spheres (PSL).

Fig. 4 shows average ± standard deviation of S'/S as a function of distance from the center of the Gaussian for (a) $D_{\mathrm{p}}=240$ nm and (b) $D_{\mathrm{p}}=600$ nm, respectively. The average and standard deviation of the Gaussian width (σ), $\bar{\sigma}$ and $\delta\sigma$, are determined by direct fitting of $S(t)$ for individual particles by the Gaussian function. The $\bar{\sigma}$ and $\delta\sigma$ are determined as the average and standard deviation of the width (σ) of the fitted Gaussian function for $\sim 10^3$ particles. The $\bar{\sigma}$ and $\delta\sigma$ values were measured to be 16.6 (0.2 μs) and 1.2 (0.2 μs), respectively, independent of D_{p} (within 1%), supporting the assumption that the particle velocity is independent of particle size. The solid line in Fig. 4 represents the I'/I line (Eq. (5)) with $\sigma=\bar{\sigma}$, and a pair of dashed lines indicate values with $\sigma=\bar{\sigma}\pm|\delta\sigma|$. In addition to Fig. 2a, results in Fig. 4 shows that the measurement by the SP2 instrument is consistent with Eqs. (4) and (5). Namely, S'/S for a non-evaporative particle (i.e., $\Delta C'_{\mathrm{sca}}=0$) equals I'/I, which is a monotonically decreasing linear function with t that only depends on the Gaussian function of incident irradiance $I(t)$. As described in Appendix A.3, the standard deviation of S'/S shown in Fig. 4 (i.e., vertical error bars) is the sum of the systematic error (Eq. (A.5)), which is caused by the variation in width of the Gaussian function, and the random error (Eq. (A.6)), which is the random error in $S(t)$. It should be noted that the systematic error equals the difference in the vertical coordinate between the solid and dashed lines in Fig. 4. The random error accounts for a large component of the vertical error bars in Fig. 4 that is not explained solely by the amplitude of the systematic error. In Figs. 4a and b, data at large distances from the center are truncated because $S(t)$ is too small, less than 3 times the resolution (i.e., 2.44 mV) of the digitizer for the $S(t)$.

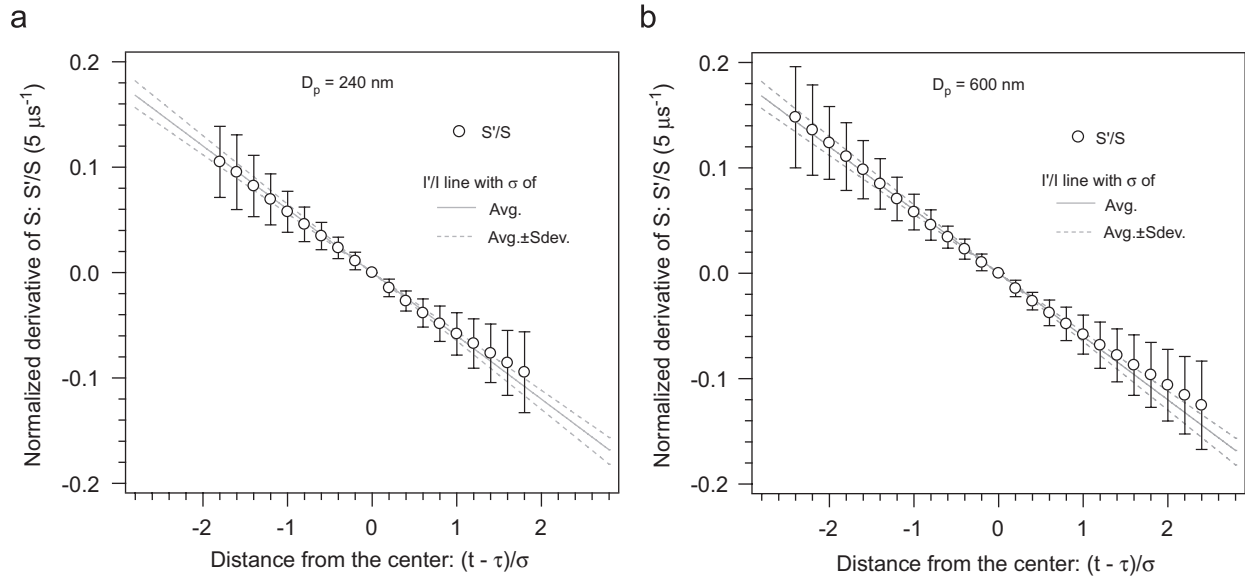

Fig. 4. Normalized derivative of scattering (S'/S) for PSL particles with (a) $D_{\mathrm{p}}=240$ nm and (b) $D_{\mathrm{p}}=600$ nm as a function of position in the Gaussian beam. Position $(t-\tau)/\sigma$ means time difference from the center of the Gaussian with units of σ. The open circles and vertical bars denote the average and ±1-standard deviation, respectively, for $\sim 10^3$ observed particles. The solid and broken lines in each figure indicate the I'/I linear functions, with $\sigma=\bar{\sigma}\pm|\delta\sigma|$.

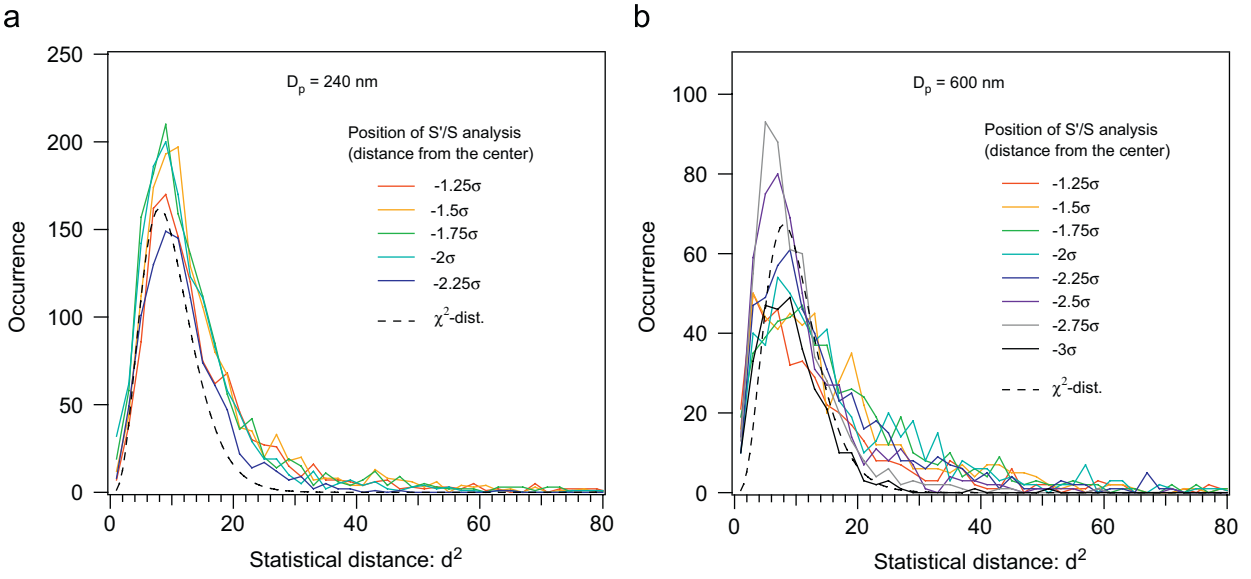

Fig. 5. Histograms of the statistical distance d^2 at various positions of S'/S analysis (positions of k) for non-evaporative PSL particles with (a) $D_p = 240$ nm and (b) $D_p = 600$ nm. Positions are indicated by the distance from the center of the Gaussian in units of σ. See Appendix A for definition of d^2. The χ^2-distribution functions are also shown for reference. The total number of observed particles is $\sim 1.5 \times 10^3$ and $\sim 0.8 \times 10^3$ for $D_p = 240$ and 600 nm, respectively.

In the t-domain of $t - \tau > 1\sigma$, S'/S systematically deviates from the I'/I line for both $D_p = 240$ and 600 nm, as shown in Fig. 4. This deviation is due to a slight distortion of the Gaussian function in $t - \tau > 1\sigma$. Because of this problem and the large computational time, analyses of S'/S are limited to the t-domain of $t - \tau < -1\sigma$.

4.2. *Position-dependent noise amplitude*

As described in Appendix A, the statistical distance between a sub-array of S'/S and the I'/I line, namely the statistical distance d^2 (Eq. (A.11)), is used to quantify the significance of whether S'/S data represent the I'/I line or not. The occurrence of d^2 for the no-evaporation condition ($\Delta C'_{sca} = 0$) follows a χ^2-distribution of $p - 1$ degrees of freedom (d.o.f.), independent of the position of the S'/S sub-array, provided that the position-dependent noise amplitude of S'/S is correctly taken into account in the d^2 calculation. Here p is the number of S'/S data points in a sub-array of S'/S (Fig. 3). The position independence of the d^2 value for the no-evaporation condition is necessary for I'/I extraction for evaporative particles, because the position of I'/I extraction varies with the timing of the onset of evaporation for individual particles.

In this study, the length of the S'/S sub-array has been set to 11, as a trade-off between the available number of data points and the statistical significance. Fig. 5 shows the occurrence of d^2 values in various positions for PSL particles, after the adjustment of parameters that determine the position-dependent noise amplitude of $S(t)$ (Eq. (A.6) in Appendix A.2). Adjustment of the parameters (A_i ($i = 1$–3) in Eq. (A.6)) is made so as to ensure that occurrences of the d^2 value for non-evaporative particles can be approximated for a χ^2-distribution with 10 d.o.f. as well as possible. By trial-and-error, optimal values of A_i ($i = 1$–3) were found to be 0.37 (units of 2.44 mV), 1.6×10^{-2} (units of $(2.44\,\text{mV})^{1/2}$), and 6.2×10^{-4}, respectively, in this study. Histograms of d^2 in Fig. 5 show that the probability distributions of d^2 become very similar to the χ^2-distribution with 10 d.o.f., independent of position and particle size. These results indicate that the χ^2-test for the d^2 value is a versatile method to judge the success of I'/I extraction from S'/S data, independent of the position of onset of evaporation and amplitude of the scattering signal.

Based on the results in Fig. 5, we use a threshold value to judge whether the sub-array of S'/S represents a segment of the I'/I line or not. We assume that a $d^2(k) < 20$ means the S'/S sub-array at position k represents the I'/I line. This classification by d^2 value is equivalent to the commonly used χ^2-test to discuss the significance of a data set sampled from the parent population of interest. As a reference, this threshold value of $d^2 = 20$ with 10 d.o.f. corresponds to the

critical level of $\alpha = 0.03$ for the χ^2-test. Namely, the number fraction of the occurrence of $d^2 < 20$ should be ~ 0.97 for non-evaporative particles if occurrence of d^2 is equal to the ideal χ^2-distribution. In reality, number fractions of $d^2 < 20$ were observed to be 0.7–0.9 for non-evaporative PSL particles (Fig. 5).

5. Validation of the $\Delta C_{sca}(t)$ measurement

To test the robustness of the method to measure $\Delta C_{sca}(t)$, we apply the method to non-evaporative particles. The center position, width, and peak amplitude of the Gaussian function estimated by the analysis of S'/S are compared to their actual values. Actual values of the parameters are determined by direct fitting of a Gaussian function onto the $S(t)$ waveform for individual particles. The peak amplitude of the Gaussian (i.e., $sI_0\Delta C_{sca}(t = \tau)$) is calculated by Eq. (3) using estimated the center position (τ) and width (σ). Comparisons between actual and estimated value of peak amplitude of the Gaussian function provide direct evidence of the validity of the $\Delta C_{sca}(t)$ estimates.

Fig. 6 shows correlations between the estimated and actual value of peak amplitude of the Gaussian function for (a) $D_p = 240$ nm and (b) $D_p = 600$ nm. Only data with $d^2 < 20$ are shown in Fig. 6 and used for the calculation of the average and standard deviation. The number fractions of particles with $d^2 < 20$ are 0.7–0.9 for D_p of both 240 and 600 nm, as discussed in Section 4.2. To show the stabilities of the estimated values of the Gaussian parameters to variations of the position of the S'/S analysis, results for different positions (k) are shown. In general, it is found from Fig. 6 that averages of the estimated and actual values of peak amplitude of the Gaussian agree accurately with each other, independent of both the position of the S'/S analysis and the particle size. These results demonstrate directly the validity of the method for estimating the $\Delta C_{sca}(t)$.

In this experiment, estimations of the Gaussian width were accurate for average values, but the standard deviations (error bars) are found to be underestimated by an order of magnitude. This discrepancy indicates that it is difficult to completely reproduce actual particle-by-particle variations of Gaussian width (σ) by our algorism. In future, to avoid this problem, it is desirable that the assumption of constant σ be applied to the algorism by reducing the fluctuation of the flow rate of the aerosol jet, as suggested in Section 3. Inaccuracies in the estimated Gaussian width (σ) do not affect the estimation of the center position (τ), because τ is determined before σ in our algorithm (Appendices A.5 and A.6).

Based on results shown in Fig. 6, uncertainty in the $\Delta C_{sca}(t)$ estimated by the S'/S analysis is estimated to be within 10%.

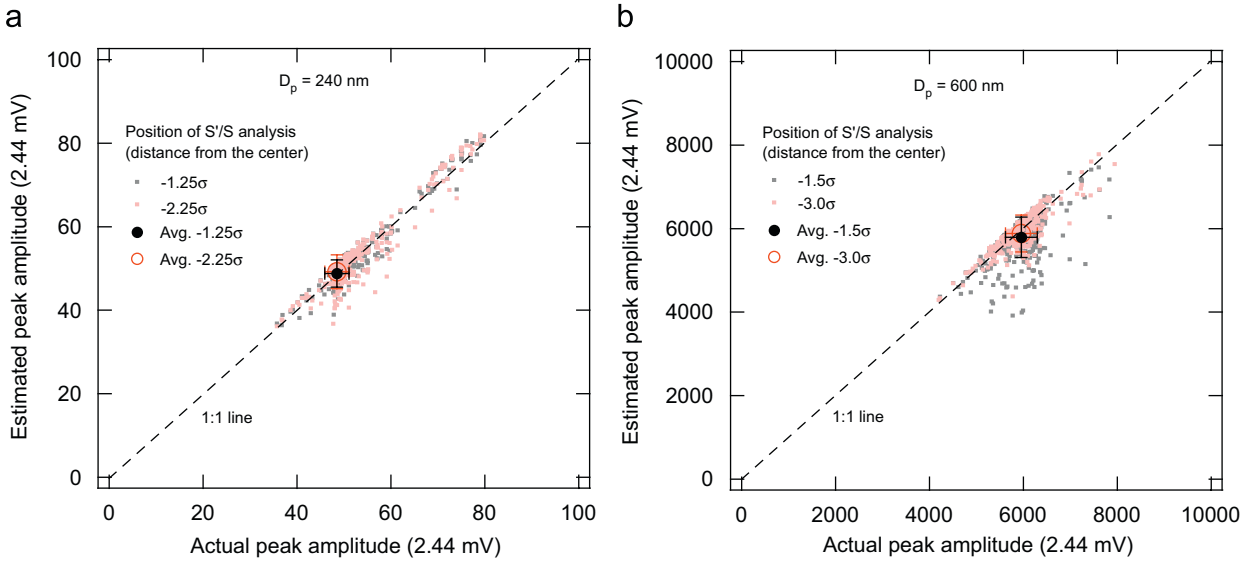

Fig. 6. Correlations between actual Gaussian amplitudes and those estimated by the S'/S analysis for non-evaporative PSL particles with (a) $D_p = 240$ nm and (b) 600 nm. Results for different positions (in σ units) of the S'/S analysis are shown. Small dots indicate data for individual particles and large circles with error bars indicate the average ± standard deviation for $\sim 10^3$ particles.

6. Measurements of evaporative particles

In this section, we show results of measurements of evaporative particles, and apply the method to estimate $\Delta C_{\mathrm{sca}}(t)$ in the laser beam. A commonly used, strongly light-absorbing test particle, nigrosin dye, did not evaporate appreciably in the SP2 laser beam under normal operating conditions. We use oil-coated graphite particles as representative evaporative particles. Oil-coated graphite particles readily evaporate in the laser beam of the SP2 due to the strong light absorption of graphite and the volatility of the coating material (Moteki & Kondo, 2007). For oil-coated graphite particles, the degree of particle evaporation can easily be varied by selecting coating materials with different thermo-chemical properties or by changing the size of the graphite core. This adjustable evaporative character of the particle is useful to test the new technique in various cases. In this study, two oils that differ from each other in evaporative character, glycerol (b.p. = 290 °C) and oleic acid (b.p. = 360 °C), have been used as coating materials.

We use commercially available colloidal graphite (stock# 41773, Alfa Aesar, Inc., Ward Hill, MA) to obtain suspended graphite particles. To generate the coated graphite particles with known core diameter (D_{c}) and particle diameter (D_{p}), we use the experimental system described by Moteki and Kondo (2007), which consists of an atomizer (Model 9032, TSI Inc., MN), two differential mobility analyzers (TSI Model 3081), and a vapor condensing system. Sheath/sample flow ratios of both DMAs are maintained in a range of 9–18, depending on the selection diameter. In this range of sheath/sample flow ratios, the size transmission width of the DMAs is narrower than ±6%. We use the mobility diameter (Hinds, 1999) as the physical definition of the particle diameter denoted by D_{p}, whereas the mass equivalent diameter (Hinds, 1999) is used as the diameter of graphite core D_{c}. For graphite particles, the mass equivalent diameter is derived from the mobility diameter based on the experimentally determined mass–mobility relation for the graphite particles (Moteki & Kondo, 2007).

6.1. Time-dependent evaporation characteristics

Fig. 7 shows typical examples of measurements for (a) glycerol and (b) oleic acid-coated graphite particle with (D_{c}, D_{p}) = (110 nm, 500 nm). These figures show time developments of scattering signal and LII signal (top), normalized derivative of scattering (S'/S) and statistical distance (d^2) (middle), and normalized incident irradiance (I/I_0) and ΔC_{sca} (bottom). The $\Delta C_{\mathrm{sca}}(t)$ value was calculated by Eq. (3) with measured scattering intensity $S(t)$ and determined Gaussian parameters (τ and σ). For glycerol-coated graphite particle, the order of the timing of scattering and the LII signal shown in the top part of Fig. 7a indicate that the coating material has completely evaporated by $t \sim 105$ followed by heating of the graphite particle to its incandescent point (T = 3000–4000 K; Moteki & Kondo, 2007) at $t > 105$. In Fig. 7a,the statistical distance d^2 continues to be about 10 at the leading edge ($45 < t < 60$) of the $S(t)$ waveform, indicating that the evaporation does not occur in this t-domain. A change in ΔC_{sca} (i.e., $\Delta C'_{\mathrm{sca}} \neq 0$) accounts for dramatic increase in d^2 at $t > 75$.

The red line depicted in the middle part of Fig. 7a indicates the I'/I function extracted from a sub-array of S'/S with the smallest d^2 (i.e., $d^2(k = k_{\mathrm{best}})$), using the numerical methods described in Appendix A. To examine the reliability of the I'/I line extraction for each particle, we use a $d^2(k_{\mathrm{best}})$ value to judge by the statistical significance that the S'/S sub-array at position $k = k_{\mathrm{best}}$ represents I'/I. As mentioned in Section 4.2, we use a threshold value of $d^2(k_{\mathrm{best}}) = 20$, which indicates the reliability of the I'/I extraction from S'/S for the particle with $d^2(k_{\mathrm{best}}) < 20$. Conversely, for a particle with $d^2(k_{\mathrm{best}}) > 20$, it is impossible to extract the I'/I line. The bottom part of Fig. 7a shows the normalized Gaussian function of $I(t)/I_0$ and $\Delta C_{\mathrm{sca}}(t)$ derived from τ and σ estimated from the extracted I'/I line. The $\Delta C_{\mathrm{sca}}(t)$ value does not change significantly at the leading edge ($t < 80$), followed by a rapid decrease at $t > 90$ due to evaporation. Results for the time-dependent particle size derived from $\Delta C_{\mathrm{sca}}(t)$ are excluded in this section to avoid complications due to optical property assumptions that are necessarily for inverting $\Delta C_{\mathrm{sca}}(t)$ to yield particle size. The relationship between particle size (D_{c}, D_{p}) and $\Delta C_{\mathrm{sca}}(t)$ for oil-coated graphite particles will be discussed exclusively in the next section. Using this relationship, the approximate time-dependent size of the particle in the laser beam can be estimated.

Fig. 7b shows results for oleic acid-coated graphite particles. In contrast to Fig. 7a (i.e., glycerol), the high intensity of $S(t)$ lasts even after the emission of the LII signal, indicating that a different evaporation phenomena occurs for this type of particle. The profile of $\Delta C_{\mathrm{sca}}(t)$ shown in the bottom part of Fig. 7b indicates that oil-coated graphite particles break up into an oil particles and a graphite particles in the laser beam. Because oleic acid is almost transparent for the incident wavelength (λ = 1064 nm), an oleic acid particle without graphite inclusion evaporates very little as a result of

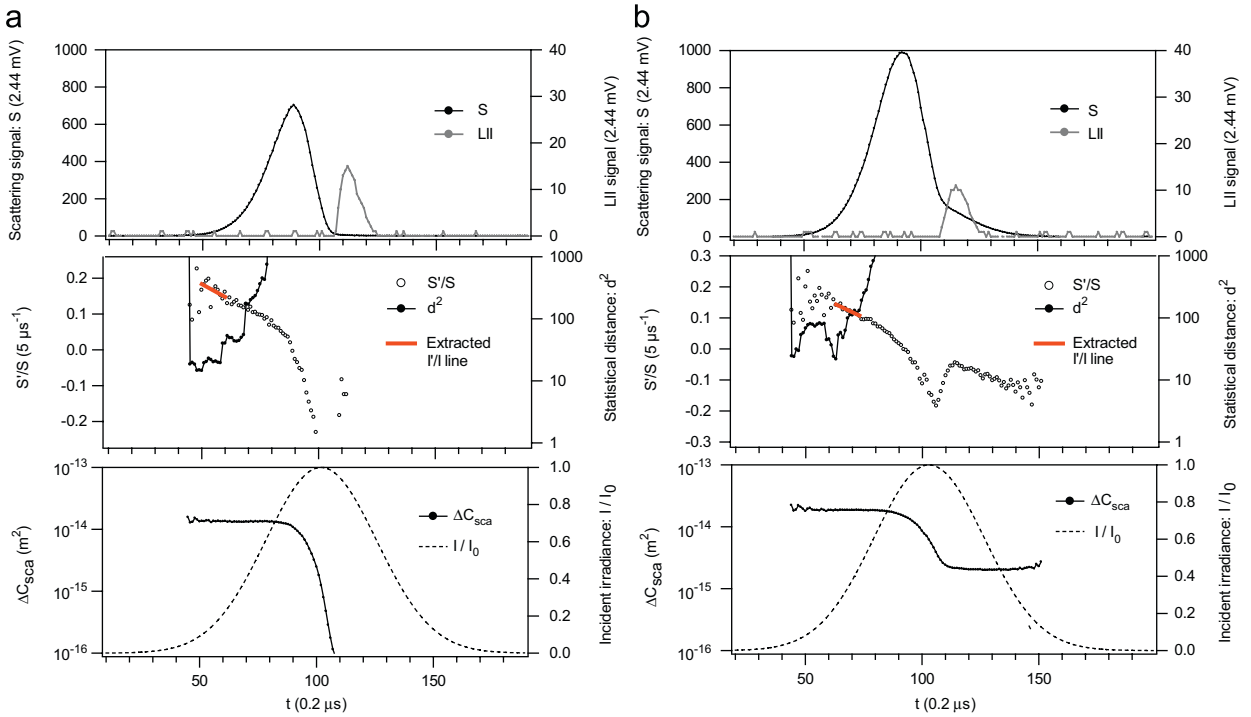

Fig. 7. Examples of the time development of important parameters for (a) glycerol and (b) oleic acid-coated graphite particles with $(D_c, D_p) = (110\,\text{nm}, 500\,\text{nm})$. The important parameters shown in these figures are: waveforms of scattering and LII signals (top); rate of change of scattering (S'/S) and the statistical distance d^2 (middle); Gaussian function of incident irradiance (normalized by I_0) and scattering cross section ΔC_{sca} (bottom). Red line segments appended on the middle figures denote the extracted I'/I functions with smallest d^2 value. Length of the line segment indicates length of sub-array of S'/S data used for statistical analysis.

laser-induced heating. Graphite cores started to incandesce at $t \sim 110$ as shown in the top part of Fig. 7b, indicating that the oleic acid coating on the graphite core disappeared (due to evaporation or disintegration) by $t \sim 110$. According to Mie calculations, scattering by a graphite core particle with a diameter of 110 nm contributes to the measured $\Delta C_{sca}(t)$ by only approximately $1 \times 10^{-17}\,\text{m}^2$. Therefore, in the time domain of $t > 110$, an observed $\Delta C_{sca}(t)$ of the order of $10^{-15}\,\text{m}^2$ cannot be explained by the graphite core. Taking into account the uncertainty in refractive index to be discussed in the next section, oleic acid particles with D_p from 300 to 400 nm can explain this observed value.

The stepwise decrease of ΔC_{sca} around $t = 100$ followed by the second plateau of ΔC_{sca} in $t > 110$ indicates that the break up of the oleic acid-coated graphite occurs at $t \sim 100$–110.

6.2. Comparison with Mie theory

6.2.1. Methods of comparison

We compare the ΔC_{sca} before the onset of evaporation (denoted ΔC^0_{sca} hereafter) with that estimated by Mie scattering theory. For a measured value of ΔC^0_{sca}, the average value of 11 continuous $(=p)$ points of $\Delta C_{sca}(t)$ at position $k = k_{best}$ are used. Results of the measurements are shown only for particles with $D_p > 300$ nm, because $S(t)$ becomes too small for the S'/S analysis of evaporative particles with $D_p < 300$ nm. The lower limits of D_p for S'/S analysis (i.e., $\Delta C_{sca}(t)$ measurements) are determined for each D_c and coating material based on examinations of the occurrence of $d^2(k_{best})$, as discussed later.

Theoretical ΔC^0_{sca} values were calculated by Mie scattering theory for internally mixed particles. The concentric shell-core model (Aden & Kerker, 1951) and volume mixture model were used for these calculations. For the volume mixture model, tiny graphite particles were assumed to be homogeneously dispersed inside the host oil droplet. Effective particle refractive indices for the volume mixture model were calculated by Maxwell-Garnet theory (Maxwell Garnett, 1904).

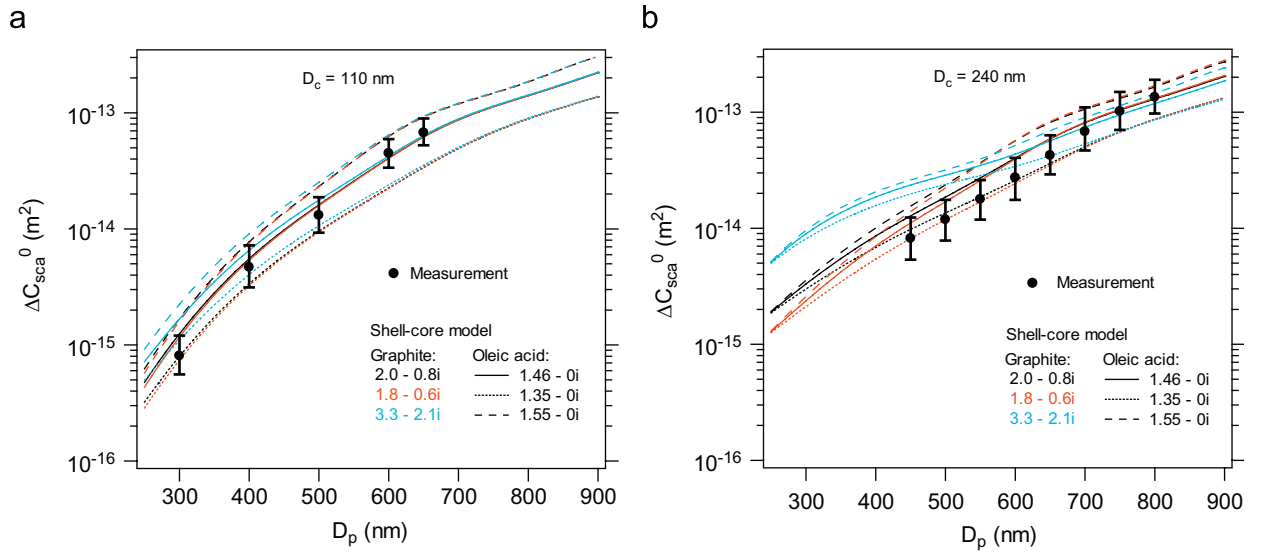

Fig. 8. Comparisons between measurement and theory for $\Delta C_{\mathrm{sca}}(t)$ before onset of evaporation ($\Delta C^0_{\mathrm{sca}}$) for oleic acid-coated graphite particles with (a) $D_{\mathrm{c}} = 110$ nm and (b) $D_{\mathrm{c}} = 240$ nm. Filled circles denote median values of each measurement for $\sim 10^3$ particles. Vertical bars indicate the ranges of 25th–75th percentile values for each measurement. Theoretical prediction curves for $\Delta C^0_{\mathrm{sca}}$ were shown for the shell-core model with various refractive indices of graphite and glycerol.

Mie calculations were made with various combinations of refractive indices of graphite and coating materials, to examine the uncertainty caused by assumed optical constants for these compounds. For refractive indices of graphite at a wavelength of 1064 nm, values of $2.0 - 0.8i$ (Howarth, Foster, & Thring, 1966) and $3.3 - 2.1i$ (Borghesi & Guizzetti, 1991) were reported for pyrographite and crystalline graphite, respectively. In addition to these values, we made calculations with the value of $1.8 - 0.6i$, which approximately equals the refractive index of propane soot at a wavelength of 1064 nm reported by Chang and Charalampopoulos (1990), as an extremely low value for the assumed refractive index of graphite. We could not find literature reports of the refractive indices of glycerol and oleic acid at infrared wavelengths. At a wavelength of 589 nm (i.e., Na-D line), refractive indices of $1.47 - 0i$ (The Chemical Society of Japan, 1993) and $1.46 - 0i$ (Japan Oil Chemists' Society, 2001) were reported for glycerol and oleic acid, respectively, and we used these values for the Mie calculations. In addition, calculations were made with coating material refractive indices of $1.35 - 0i$ and $1.55 - 0i$ to examine the sensitivity of the results to the uncertainty in the wavelength dependences of the refractive indices.

The Mie scattering codes of BHCOAT and BHMIE (Bohren & Huffman, 1983) were used for calculations with the shell-core model and volume mixture model, respectively. For the ranges of D_{c} and D_{p} measured in this experiment, the differences in $\Delta C^0_{\mathrm{sca}}$ calculated by the shell-core and volume mixture models were found to be only several percent for the fixed values of refractive indices of graphite and coating materials. Several-percent differences in $\Delta C^0_{\mathrm{sca}}$ are small compared to the difference caused by changing the assumed value of the refractive index. Therefore, we show only the results for the shell-core model.

6.2.2. *Oleic acid-coated graphite particles*

Fig. 8 shows measured and theoretical $\Delta C^0_{\mathrm{sca}}$ of oleic acid-coated graphite particles with (a) $D_{\mathrm{c}} = 110$ and (b) 240 nm. Corresponding to the measurements shown in Fig. 8, histograms of the statistical distance at the position of the S'/S analysis, namely, $d^2(k = k_{\mathrm{best}})$, are shown in Fig. 9. As an exception, significant deviations of $d^2(k_{\mathrm{best}})$ from the χ^2-distribution are observed for $D_{\mathrm{p}} \leqslant 350$ nm. These deviations are due to the lack of $S(t)$ data points with a sufficient signal-to-noise ratio before the onset of evaporation. Furthermore, other results from the measurement of oleic acid-coated graphite particles are summarized in Table 1. The $\Delta C^0_{\mathrm{sca}}$ data points in Fig. 8 are for particles with $d^2(k_{\mathrm{best}}) < 20$, whereas Fig. 9 shows results for all particles.

As shown in Fig. 9, for a majority of the measurements, the occurrence of $d^2(k_{\mathrm{best}})$ is very similar to the χ^2-distribution (with 10 d.o.f.) as well as the results for PSL (Fig. 5). This fact indicates that the I'/I lines are reliably extracted from

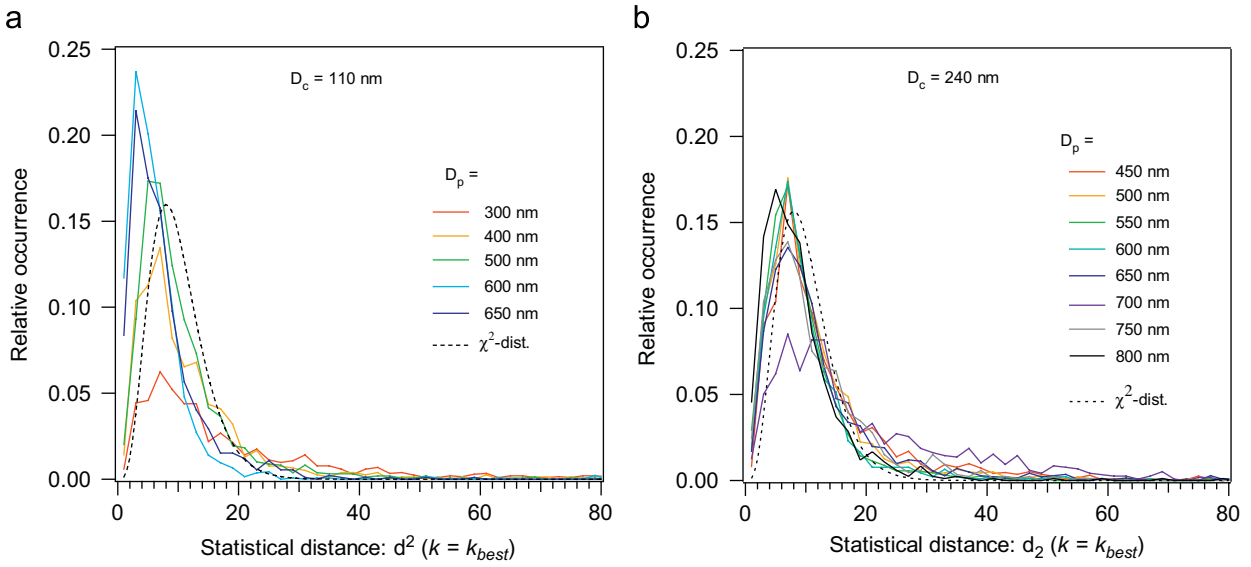

Fig. 9. Histograms of the statistical distance d^2 at the position of I'/I line extraction for oleic acid-coated graphite particles with (a) $D_c = 110$ nm and (b) $D_c = 240$ nm. Results shown in these figures correspond to those shown in Fig. 8. The χ^2-distribution functions with 10 degrees of freedom are also shown for reference. The amplitudes of these χ^2-distribution functions are not important.

Table 1
Summary for oleic-acid coated graphite particles

D_p (nm)	Total number of observation	Position of S'/S analysis (σ)	Number fraction of $d^2(k_{best}) < 20$	Estimated Gaussian width σ (0.2 μs)	Median value of the ratio $\Delta C_{sca}(t = \tau)/\Delta C^0_{sca}$
(a) $D_c = 110$ nm					
300	2052	-2.3 ± 0.3	0.36	16.6 ± 0.2	0
400	780	-2.8 ± 0.3	0.68	16.6 ± 0.12	0.03
500	1587	-3.1 ± 0.3	0.83	16.6 ± 0.10	0.68
600	1359	-2.4 ± 0.6	0.92	16.6 ± 0.11	0.88
650	920	-2.5 ± 0.6	0.88	16.6 ± 0.11	0.94
(b) $D_c = 240$ nm					
450	1950	-3.1 ± 0.3	0.77	16.6 ± 0.11	0.02
500	1827	-3.2 ± 0.2	0.83	16.6 ± 0.10	0.03
550	1949	-3.3 ± 0.3	0.82	16.6 ± 0.10	0.18
600	915	-3.3 ± 0.4	0.79	16.6 ± 0.10	0.44
650	1418	-2.9 ± 0.8	0.75	16.6 ± 0.12	0.70
700	1175	-2.7 ± 0.8	0.55	16.6 ± 0.14	0.85
750	865	-2.7 ± 0.7	0.78	16.6 ± 0.12	0.98
800	839	-2.6 ± 0.8	0.86	16.6 ± 0.12	0.99

(a) Results shown in this table correspond to those shown in Figs. 8a and 9a.
(b) Results shown in this table correspond to those shown in Figs. 8b and 9a.

S'/S for a majority of these measurements. Successes of I'/I extraction ensure reliable $\Delta C_{sca}(t)$ measurements, as demonstrated by the analysis of non-evaporative particle in Section 5.

Fig. 8 shows that systematic deviations of the theoretical curves from the measurements are moderately small (i.e., within 30%) in the case of the graphite refractive indices of $2.0 - 0.8i$ or $1.8 - 0.6i$ and $1.46 - 0i$ or $1.35 - 0i$ for oleic acid.

Table 1 shows the median values of the ratio of $\Delta C_{sca}(t = \tau)$ (i.e., ΔC_{sca} at the center of the laser beam) to ΔC^0_{sca} ($\Delta C_{sca}(t = \tau)/\Delta C^0_{sca}$), as an indicator of degree of evaporation of the particles. For particles with small a D_p/D_c ratio, particle tends to evaporate rapidly inside the laser beam, as indicated by the small $\Delta C_{sca}(t = \tau)/\Delta C^0_{sca}$. In contrast, particles with large D_p/D_c ratios evaporate very little inside the laser beam, as indicated by $\Delta C_{sca}(t = \tau)/\Delta C^0_{sca}$ values close to unity. The estimated Gaussian width σ (only for particles with $d^2(k_{best} < 20)$) is also summarized in Table 1.

The average values of the estimated σ accurately agree with that of non-evaporative particles (i.e., 16.6 μs). However, the standard deviations of σ are estimated to be an order of magnitude less than that of the actual σ, as well as in the case of non-evaporative particles discussed in Section 5.

6.2.3. Glycerol-coated graphite particles

The degree of evaporation for glycerol-coated graphite is significantly higher than that for oleic acid-coated graphite with the same D_c and D_p, indicating significant differences in the evaporative characters of these coating materials. This difference corresponds to the phenomenon that oleic acid-coated graphite particles are more likely to break up into core and shell than in the case of glycerol, as shown in Fig. 7a and b.

As in the case of oleic acid, for a majority of the measurements the occurrences of $d^2(k_{best})$ are very similar to the χ^2-distribution (of 10 d.o.f.) for $D_P > 350$ nm. The systematic deviations of the theoretical curves from the measurements are moderately small (i.e., within 50%) in the case of graphite refractive indices of $2.0-0.8i$ or $1.8-0.6i$ and $1.35-0i$ for glycerol.

7. Summary

A new method for measuring the time-dependent solid angle scattering cross section for detection ($\Delta C_{sca}(t)$) of aerosol particles in a laser beam has been developed. This method is based on the principle that the normalized derivative of the scattering signal (S'/S) measured by the scattering probe can be decomposed into the normalized derivative of the incident laser irradiance (I'/I) and that of the scattering cross section ($\Delta C'_{sca}/\Delta C_{sca}$). The present formulation predicts that, for non-evaporative particles, $S'/S = I'/I$, because $\Delta C'_{sca} = 0$, as has been verified by laboratory experiment. For evaporative particle, $S'/S = I'/I$ also holds until evaporation starts. $I(t)$ for individual evaporative particles, which is usually unknown, can be deduced from the S'/S data at the leading edge of $S(t)$ by the statistical method developed. $\Delta C_{sca}(t)$ is derived from Eq. (3) using derived $I(t)$ and observed $S(t)$. The validity of this method was confirmed by comparisons between estimated and actual values of the parameters that characterize $I(t)$ for non-evaporative particles by using a DMT single-particle soot photometer (SP2).

The $\Delta C_{sca}(t)$ of individual evaporative particles (i.e., glycerol or oleic acid-coated graphite) has been derived, demonstrating the usefulness of the method to monitor the evaporation phenomena of individual particles. $\Delta C_{sca}(t)$ values before the onset of evaporation (ΔC^0_{sca}) were compared to those predicted by Mie scattering theory. Although the predicted results are highly sensitive to the assumed refractive indices of both graphite and coating materials, moderately good agreements (to within 50%) were observed for some assumed ranges of refractive indices. The lower limit of particle diameter for $\Delta C_{sca}(t)$ estimation is about 400 nm for the present instrumentation, because the scattering signal becomes too small for smaller particle sizes.

Several important improvements to the measurement of $\Delta C_{sca}(t)$ would reduce the uncertainty. First, reducing the fluctuation of the flow velocity of the carrier gas is critical in stabilizing the width of Gaussian function $I(t)$. Stabilization of the width enables us to assume a constant width for the analysis, significantly simplifying the numerical method of analysis. This simplification avoids the problem of erroneous estimation of the Gaussian width of individual particles appearing in this study. Secondly, it is critical to use a high-quality laser beam whose transverse mode is close to the ideal Gaussian with low noise. Finally, detection of $S(t)$ within a wider range of positions (e.g., up to $t < -4\sigma$) in the laser beam will increase the available data for the S'/S analysis, especially for highly evaporative particles.

Acknowledgments

This work is supported by the Japan Society for the Promotion of Science (JSPS). We thank M. Shiraiwa for reviewing the numerical scheme and sharing experimental results for nigrosin dye test particles. We are indebted to J.P. Schwarz for useful comments.

Appendix A.

A.1. Normalized derivative of the scattering signal

The time derivative of $S(t)$ is approximated by the 4th order central difference (e.g., Jaluria & Torrance, 2003),

$$S'(t_i) \equiv S'_i \approx \frac{-S_{i+2} + 8S_{i+1} - 8S_{i-1} + S_{i-2}}{12h}, \tag{A.1}$$

where h indicates the time resolution of the $S(t)$ measurement, namely $t_{i+1} = t_i + h$. From Eq. (A.1), the normalized derivative of the scattering signal $S'/S(t_i)$ (denoted by y_i for simplicity) becomes

$$\frac{S'_i}{S_i} = \frac{1}{12h}\frac{-S_{i+2} + 8S_{i+1} - 8S_{i-1} + S_{i-2}}{S_i}. \tag{A.2}$$

A.2. Numerical methods for S'/S analysis

A brief explanation of the numerical algorism to estimate $\Delta C_{\mathrm{sca}}(t)$ is given in this section. First of all, we set the length of the sub-array of S'/S and scanning range of k, namely p and k_{end}. In Section A.3, a statistical model for a single S'/S data point is described. The statistical model includes experimental parameters (σ, $\delta\sigma$, A_1, A_2, and A_3) that are determined by the measurement of non-evaporative particles. Based on this model, we formulate a statistical model for a S'/S sub-array with $\Delta C'_{\mathrm{sca}} = 0$ in Section A.4. Numerical methods to determine the $\Delta C_{\mathrm{sca}}(t)$ of evaporative particles are based on the sub-array model. In Section A.5, numerical methods to determine the center of the Gaussian τ and to evaluate the statistical significance of each S'/S sub-array is introduced. Then, we conduct a statistical test for the chosen S'/S sub-array to examine whether the sub-array represents a segment of the I'/I line. Finally, the method to determine the width of the Gaussian σ is described in Section A.6.

A.3. Statistical model for a S'/S data point with $\Delta C'_{\mathrm{sca}} = 0$

Hereafter, we denote S'/S and y interchangeably for simplicity. Provided $\Delta C'_{\mathrm{sca}} = 0$, the behavior of the normalized derivative of scattering (y) at time t_i can be expressed as the sum of the average value $\bar{y}_i$, systematic error $(\delta y_i)_{\mathrm{sys}}$, and random error $(\delta y_i)_{\mathrm{ran}}$,

$$y_i = \bar{y}_i + (\delta y_i)_{\mathrm{sys}} + (\delta y_i)_{\mathrm{ran}} \quad \text{where } \Delta C'_{\mathrm{sca}}(t_i) = 0, \tag{A.3}$$

where δ denotes the error of the variable, with a typical value $\pm$ standard deviation. Formulations of $\bar{y}_i$, $(\delta y_i)_{\mathrm{sys}}$ and $(\delta y_i)_{\mathrm{ran}}$ as functions of known parameters are necessary to specify the statistical model of y_i (Eq. (A.3)).

First, $\bar{y}_i$ equals to right-hand side (RHS) of Eq. (5), with the average width ($\bar{\sigma}$) of the Gaussian function,

$$\bar{y}_i = -\frac{1}{\bar{\sigma}^2}(t_i - \tau). \tag{A.4}$$

It must be noted that the τ is an unknown parameter that has to be determined by the method to be introduced in Section A.5.

Secondly, the systematic error in y_i ($(\delta y_i)_{\mathrm{sys}}$) is caused by the random fluctuation in the width (σ) of the Gaussian function, which is due to the fluctuation in the flow rate of the aerosol jet,

$$(\delta y_i)_{\mathrm{sys}} = \frac{\partial}{\partial\sigma}\left(\frac{I'}{I}\right)_{\sigma=\bar{\sigma}}\delta\sigma = \frac{2}{\bar{\sigma}^3}(t_i - \tau)\delta\sigma. \tag{A.5}$$

In this equation, the random variable $\delta\sigma$ is constant and independent of i. Eq. (A.5) shows that the amplitude of $(\delta y_i)_{\mathrm{sys}}$ is linearly proportional to the distance from the center of the Gaussian ($t_i - \tau$). The values of $\bar{\sigma}$ and $\delta\sigma$ in Eqs. (A.4) and (A.5) are determined by the observation of non-evaporating particles in the laboratory, as detailed in Section 4.1.

Thirdly, the random error in y_i ($(\delta y_i)_{\mathrm{ran}}$) originates from the random error (δS_i) in the measurement of S_i. For simplicity, we neglect the frequency dependence of the noise amplitude. In this study, we use the following mathematical model of the noise amplitude δS_i,

$$\delta S_i = \pm\sqrt{A_1^2 + A_2^2 \cdot S_i + A_3^2 \cdot S_i^2}, \tag{A.6}$$

where A_i ($i = 1$–3) are constants determined experimentally. The fist term on the RHS of Eq. (A.6) represents the noise component independent of signal intensity (e.g., quantization error, thermal noise), and the second and third term represents noise components proportional to the square root of the signal intensity (e.g., shot noise) and the signal intensity itself (e.g., laser noise), respectively. An experimental method for estimating parameters A_i ($i = 1$–3)

is detailed in Section 4.2. The random error in y_i ($(\delta y_i)_{\mathrm{ran}}$) relates to δS_i as follows. From Eq. (A.2), the random error in y_i is calculated considering the law of propagation of independent errors (Bevington & Robinson, 2003),

$$
\begin{aligned}
&(\delta y_i)_{\mathrm{ran}} \\
&= \sqrt{\left(\frac{\partial y_i}{\partial S_i}\right)^2 \delta S_i^2 + \left(\frac{\partial y_i}{\partial S_{i+2}}\right)^2 \delta S_{i+2}^2 + \left(\frac{\partial y_i}{\partial S_{i-2}}\right)^2 \delta S_{i-2}^2 + \left(\frac{\partial y_i}{\partial S_{i+1}}\right)^2 \delta S_{i+1}^2 + \left(\frac{\partial y_i}{\partial S_{i-1}}\right)^2 \delta S_{i-1}^2} \\
&= \frac{1}{12h}\sqrt{\left(\frac{-S_{i+2}+8S_{i+1}-8S_{i-1}+S_{i-2}}{S_i^2}\right)^2 \delta S_i^2 + \left(\frac{-1}{S_i}\right)^2 \delta S_{i+2}^2 + \left(\frac{1}{S_i}\right)^2 \delta S_{i-2}^2 + \left(\frac{8}{S_i}\right)^2 \delta S_{i+1}^2 + \left(\frac{-8}{S_i}\right)^2 \delta S_{i-1}^2} \\
&\approx \frac{\sqrt{130}}{12} \cdot \frac{1}{h} \cdot \frac{1}{S_i} \cdot \delta S_i = \frac{A_{fd}}{h} \cdot \frac{1}{S_i} \cdot \delta S_i, \qquad \text{(A.7)}
\end{aligned}
$$

where A_{fd} is constant, depending only on the numerical scheme of the finite difference approximation of S' (Eq. (A.1)), and h is the time resolution of the data points, which is the same as the inverse of the sampling rate of the digitizer (i.e., 0.2 μs).

From Eqs. (A.3)–(A.5), and (A.7), y_i can be expressed as

$$
y_i = -\frac{1}{\bar{\sigma}^2}(t_i - \tau) + \frac{2}{\bar{\sigma}^3}(t_i - \tau) \cdot \delta\sigma + \frac{A_{fd}}{h}\frac{1}{S_i} \cdot \delta S_i \quad \text{where } \Delta C'_{\mathrm{sca}}(t_i) = 0. \qquad \text{(A.8)}
$$

Eq. (A.8) is a statistical model of each data point of y_i with $\Delta C'_{\mathrm{sca}} = 0$. This equation means that the two elementary random variables $\delta\sigma$ and δS_i account for the statistical variation of y_i. The amplitude of $\delta\sigma$ is independent of i, whereas that of δS_i randomly changes with i.

A.4. Statistical model of a sub-array of S'/S with $\Delta C'_{\mathrm{sca}} = 0$

Here, the kth set of p data points of y_i (i.e., sub-array of y) is chosen, and a statistical analysis is conducted on this sub-array. We need a parent population of the p-dimensional data for the statistical analysis. The parent population is formulated as a p-dimensional multivariate normal distribution, taking into account the variance and covariance of the y data points. This formulation is based on the statistical model of each data point developed in the previous section. The probability of observing an arbitrary sub-array from the parent population of I'/I (i.e., y with $\Delta C'_{\mathrm{sca}} = 0$) can be described as a multivariate normal distribution of the p-dimension,

$$
L_k(\tau) = \frac{1}{(\sqrt{2\pi})^p |\Sigma_k|^{1/2}} \exp\left[-\frac{1}{2}(\mathbf{y}_k - \bar{\mathbf{y}}_k)^{\mathrm{t}} \Sigma_k^{-1} (\mathbf{y}_k - \bar{\mathbf{y}}_k)\right], \qquad \text{(A.9)}
$$

where the symbol $|\ |$ and the superscript -1 denote the determinant and inverse of the matrix, respectively. In Eq. (A.9), $\mathbf{y}_k$ and $\bar{\mathbf{y}}_k$ denote p-dimensional vectors of y and $\bar{y}$ (i.e., Eq. (A.4)) for the kth sub-array, respectively,

$$
\mathbf{y}_k = \begin{pmatrix} y_k \\ y_{k+1} \\ \vdots \\ y_{k+p-1} \end{pmatrix}, \quad \bar{\mathbf{y}}_k = -\frac{1}{\bar{\sigma}^2} \begin{pmatrix} t_k - \tau \\ t_{k+1} - \tau \\ \vdots \\ t_{k+p-1} - \tau \end{pmatrix}.
$$

And Σ_k in Eq. (A.9) is the p-dimensional variance-covariance matrix of the data vector $\mathbf{y}_k$,

$$
\Sigma_k = \begin{pmatrix} Var[y_k] & Cov[y_k, y_{k+1}] & \cdots & Cov[y_k, y_{k+p-1}] \\ Cov[y_{k+1}, y_k] & & & \\ & \ddots & & \\ \vdots & & & \vdots \\ & & & \\ Cov[y_{k+p-1}, y_k] & \cdots & & Var[y_{k+p-1}] \end{pmatrix},
$$

where the variance of y_i and the covariance between y_i and y_j $(i \neq j)$ are derived from Eq. (A.8) as follows:

$$Cov[y_i, y_j] = \frac{4}{\bar{\sigma}^6}(t_i - \tau)(t_j - \tau) \cdot \delta\sigma^2, \tag{A.10a}$$

$$Var[y_i] = \frac{4}{\bar{\sigma}^6}(t_i - \tau)^2 \cdot \delta\sigma^2 + \frac{A_{fd}^2}{h^2}\frac{1}{S_i^2} \cdot \delta S_i^2. \tag{A.10b}$$

As a means to derive Eq. (A.10) from Eq. (A.8), Johnson and Wichern (2007) show a derivation of variance and covariance of secondary statistical variables that is a linear combination of multiple random variables. The square root of the quadratic form in Eq. (A.9), namely

$$d(k) = \sqrt{(\mathbf{y}_k - \bar{\mathbf{y}}_k)^{\mathrm{t}} \Sigma_k^{-1} (\mathbf{y}_k - \bar{\mathbf{y}}_k)} \tag{A.11}$$

is called the statistical distance (Johnson & Wichern, 2007; Mahalanobis, 1936). The $d(k)$ value is a measure of the distance between $\mathbf{y}_k$ and $\bar{\mathbf{y}}_k$ in p-dimensional space, taking into account both the variance and covariance of the elements in $\mathbf{y}_k$. Values of d are generally small in the interior and large outside the parent population.

A.5. Determination of the center of the Gaussian: τ

The unknown parameter τ in Eq. (A.9) is determined so as to maximize $L_k(\tau)$ for each k. The maximum-likelihood estimation (Bevington & Robinson, 2003) of τ is conducted for each k (i.e., $k = 0 \sim k_{\mathrm{end}}$). Because it is impossible to obtain the τ that maximizes $L_k(\tau)$ analytically, the maximum of the $L_k(\tau)$ is numerically derived by a grid-search method (Bevington & Robinson, 2003) with respect to a one-dimensional parameter space of τ. After the determination of τ for each k, the most statistically significant τ (τ_{best}) has to be selected over the 1-dimensional parameter space of k. The k corresponding to τ_{best} is denoted k_{best} hereafter. For the purpose of determining k_{best}, the $d^2(k)$ value can be used as a measure of the statistical significance. The k_{best} for the particle is determined so as to minimize the $d^2(k)$ value over the 1-dimensional parameter space of k.

After the determination of k_{best}, it is necessary to ensure that the k_{best}th sub-array of y has been sampled from the interior of the parent population with $\Delta C'_{\mathrm{sca}} = 0$. The probability of occurrence of $d^2(k)$ follows the χ^2-distribution of $p - 1$ d.o.f., considering that 1-parameter (τ) fitting has been conducted on the p-dimensional data. Therefore, the χ^2-test of $p - 1$ d.o.f. using the $d^2(k_{\mathrm{best}})$ value is useful in order to examine whether or not the k_{best}th sub-array of y belongs to the parent population with $\Delta C'_{\mathrm{sca}} = 0$.

A.6. Estimating the width of the laser beam: σ

In this section, we determine the width of the Gaussian σ using the k_{best} and τ_{best} already determined. For the determination of σ, the slope of the linear I'/I function $(-1/\sigma^2)$ is determined by the weighted least-squares fitting (Bevington & Robinson, 2003) of a linear function of the k_{best}th sub-array of y. The weighted least-squares fitting to estimate the slope (a) of the linear function reduces to minimizing the following function:

$$f(a) = \sum_{i=k_{\mathrm{best}}}^{p} \left[\frac{\{y_i - a(t_i - \tau_{\mathrm{best}})\}^2}{(\delta y_i)_{\mathrm{ran}}^2} \right], \tag{A.12}$$

where $1/(\delta y_i)_{\mathrm{ran}}^2$ is the weighting of the ith data point. The condition $\partial f/\partial a = 0$ gives the a that minimize f as

$$a = -\sum_{i=k_{\mathrm{best}}}^{p} \left[\frac{(\tau_{\mathrm{best}} - t_i) y_i}{(\delta y_i)_{\mathrm{ran}}^2} \right] \Bigg/ \sum_{i=k_{\mathrm{best}}}^{p} \left[\frac{(\tau_{\mathrm{best}} - t_i)^2}{(\delta y_i)_{\mathrm{ran}}^2} \right] \tag{A.13}$$

and $\sigma = (-1/a)^{1/2}$.

Finally, the $I(t)$ and the $\Delta C_{\mathrm{sca}}(t)$ for individual particle can be calculated by Eqs. (1) and (3), respectively, using the determined parameters τ and σ.

References

Aden, A. L., & Kerker, M. (1951). Scattering of electromagnetic waves from two concentric spheres. *Journal of Applied Physics*, *22*, 1242–1246.

Baumgardner, D., Kok, G., & Raga, G. (2004). Warming of Arctic lower stratosphere by light absorbing particles. *Geophysical Research Letters*, *31*, L06117.

Bevington, P. R., & Robinson, D. K. (2003). *Data reduction and error analysis for the physical sciences*. (3rd ed.), New York: McGraw-Hill.

Bohren, C. F., & Huffman, D. R. (1983). *Absorption and scattering of light by small particles*. New York: Wiley.

Borghesi, A., & Guizzetti, G. (1991). Graphite (C). In E. D. Palik (Ed.), *Handbook of optical constants of solids II.* New York: Academic Press.

Chang, H., & Charalampopoulos, T. T. (1990). Determination of the wavelength dependence of refractive indices of flame soot. *Proceedings Royal Society, Series A*, *430*(1880), 577–591.

Gao, R. S., Schwarz, J. P., Kelly, K. K., Fahey, D. W., Watts, L. A., Thompson, T. L. et al. (2007). A novel method for estimating light-scattering properties of soot Aerosols using a modified single-particle soot photometer. *Aerosol Science and Technology*, *41*, 125–135.

Hinds, W. C. (1999). *Aerosol technology*. (2nd ed.), New York: Wiley.

Howarth, C. R., Foster, P. J., & Thring, M. W. (1966). The effect of temperature on the extinction of radiation by soot particles. In *Proceedings of the third international heat transfer conference* (Vol. 5, pp. 122–128). Washington, D.C: Hemisphere.

Jaluria, Y., & Torrance, K. E. (2003). *Computational heat transfer* (2nd ed.). Appendix A. NY: Taylor & Francis.

Japan Oil Chemists' Society (Ed.). (2001). Lipid and surfactants. In *Handbook of oil chemistry* (4th ed.). Tokyo, Japan: Maruzen.

Johnson, R. A., & Wichern, D. W. (2007). *Applied multivariate statistical analysis*. (6th ed.), NJ: Pearson Education, Inc.

Kerker, M. (1997). Light scattering instrumentation for aerosol studies: An historical overview. *Aerosol Science and Technology*, *27*, 522–540.

Mahalanobis, P. C. (1936). On the generalised distance in statistics. *Proceedings of the National Institute of Science of India*, *12*, 49–55.

Maxwell Garnett, J. C. (1904). Colours in metal glasses and in metallic films. *Philosophical Transactions of the Royal Society of London*, *A203*, 385–420.

Moteki, N., & Kondo, Y. (2007). Effects of mixing state of black carbon measurement by laser-induced incandescence. *Aerosol Science and Technology*, *41*, 398–417.

Pinnick, R. G., Pendleton, J. D., & Videen, G. (2000). Response characteristics of the particle measuring systems active scattering aerosol spectrometer probes. *Aerosol Science and Technology*, *33*, 334–352.

Schoolcraft, T. A., Constable, G. S., Zhigilei, L. V., & Garrison, B. J. (2000). Molecular dynamics simulation of the laser disintegration of aerosol particles. *Analytical Chemistry*, *72*, 5143–5150.

Schulz, C., Kock, B. F., Hofmann, M., Michelsen, H., Will, S., Bougie, B. et al. (2006). Laser-induced incandescence: Recent trends and current questions. *Applied Physics B*, *83*, 333–354.

Schuster, B. G., & Knollenberg, R. (1972). Detection and sizing of small particles in an open cavity gas laser. *Applied Optics*, *11*, 1515–1520.

Schwarz, J. P., Gao, R. S., Fahey, D. W., Thomson, D. S., Watts, L. A., Wilson, J. C. et al. (2006). Single-particle measurement of mid latitude black carbon and light-scattering aerosols from the boundary layer to the lower stratosphere. *Journal of Geophysical Research*, *111*, D16207.

Sleicher, C. A., & Churchill, S. W. (1956). Radiant heating of dispersed particles. *Industrial and Engineering Chemistry*, *48*, 1819–1824.

Slowik, J. G., Cross, E. S., Han, J.-H., Davidovits, P., Onasch, T. B., Jayne, J. T. et al. (2007). An inter-comparison of instruments measuring black carbon content of soot particles. *Aerosol Science and Technology*, *41*, 295–314.

Stephens, M., Turner, N., & Sandberg, J. (2003). Particle identification by laser-induced incandescence in a solid-state laser cavity. *Applied Optics*, *42*, 3726–3736.

The Chemical Society of Japan (Ed.). (1993). *Handbook of chemistry* (Basic fourth ed.). Tokyo, Japan: Maruzen.